MÖSSBAUER SPECTROSCOPY
NEWSLETTER

April 2025

Development of Fe^{II} Tetranuclear Cages: Spin Crossover and Their Ammonia Sensing Application

Weiyang Li, Yann Garcia (✉)
Institute of Condensed Matter and Nanosciences, Molecular Chemistry, Materials and Catalysis (IMCN/MOST), Université catholique de Louvain, Place Louis Pasteur 1, 1348 Louvain-la-Neuve, Belgium
Email: yann.garcia@uclouvain.be

Table of Contents:

I. Introduction and context
II. 1. First SCO $Fe^{II}_4L_6$ cage based on pyridyl-hydrazone sites
III. 2. SCO in a family of $Fe^{II}_4L_6$ cages with pyridyl-hydrazone ligand scaffolds modulated by solvents, counter anions and substituents
IV. 3. From a mononuclear $Fe^{II}L_2$ complex to a SCO $Fe^{II}_4L_6$ cage for colorimetric ammonia sensing
V. 4. A SCO $Fe^{II}_4L_4$ cage for fast ammonia sensing and the monitoring pork spoilage
VI. General conclusions
VII. Acknowledgments
VIII. References

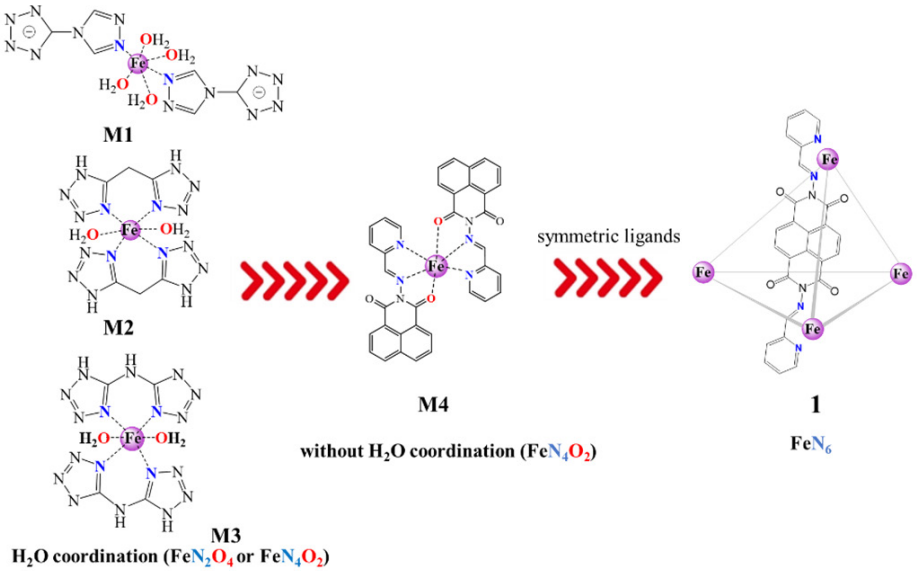
The 4803 issue mainly published the parts of the Forth section **3. From a mononuclear $Fe^{II}L_2$ complex to a SCO $Fe^{II}_4L_6$ cage for colorimetric ammonia sensing** to the last section **References**

3. From a mononuclear $Fe^{II}L_2$ complex to a SCO $Fe^{II}_4L_6$ cage for colorimetric ammonia sensing

The application of Fe^{II} SCO cages in the solid state is in its infancy and is limited to the adsorption of guest molecules as porous adsorbents. In this section, we will investigate the potential application of Fe^{II} supramolecular cage (**1**) for ammonia sensing. Recently, our group developed three Fe^{II} mononuclear complexes (**M1-M3**, **Scheme 3**), which were able to colorimetric detect various toxic volatile chemicals under ambient conditions, but with a slower response to $NH_{3(g)}$ due to non-porosity [23-27, 38]. The discoloration mechanism is ascribed to the substitution of coordinated water by guest $NH_{3(g)}$ molecules leading to a change in the Fe^{II} spin state from complete HS to a mixed HS/LS situation [23-27, 38]. To improve the response time of Fe^{II}-based sensors for $NH_{3(g)}$ as well as to investigate the sensing mechanism of different Fe^{II}-based sensors (featuring various coordination modes), we prepared a mononuclear HS complex **M4** and cage **1** by symmetric modification of the ligand structure (**Scheme 3**).

To quantitatively compare the color change of **M4** after exposure to $NH_{3(g)}$, we explored the conversion of colour information into numerical values, *i.e.* Euclidean distance, which is calculated based on six-dimensional color vectors including RGB (red, green, and blue) and HSB1 (hue, saturation, and brightness) extracted from digital images taken by a smartphone [40]. When the native **M4** is in contact with ammonia vapor at room temperature, it turned from reddish brown to dark grey in 8 min and kept its final color after 15 min (**Figure 7**). The diffuse reflectance spectrum of **M4** showed a broad band around λ = 535 nm, which is attributed to metal-to-ligand charge transfer (MLCT) processes [23, 24]. A clear shift of the band centered at about λ = 580 nm can be observed in **M4**@NH_3, which is probably due to the $^1A_1 \rightarrow {}^1T_1$ *d–d* transition of the LS state of Fe^{II} ions [23, 24].

The ^{57}Fe Mössbauer spectrum of **M4** at 298 K exhibited a single doublet [δ =



Scheme 3. Structures of three reported mononuclear Fe^{II}-based sensors [23-27, 38] and the new designed Fe^{II}-based sensors (**M4** and **1**) [39].

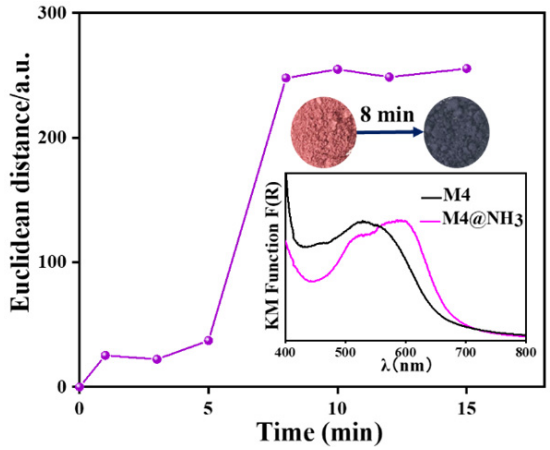


Figure 7. Response time curve of **M4** to $NH_{3(g)}$ under vapor diffusion at room temperature. Inset: diffuse reflectance spectrum and digital images of **M4** and **M4**@NH_3 (exposure for 8 min), KM = Kubelka-Munk [39].

1.00(1) mm s^{-1}; ΔE_Q = 2.56(2) mm s^{-1}], corresponding to typical HS Fe^{II} ions, with an area fraction (A) of 100% (**Figure 8a**). Similar Mössbauer parameters can be found in other Fe^{II} complexes with tridentate Schiff base ligands with *N,N,O* donor sets [41, 42]. The slight observed asymmetry of the peaks is presumably due to the preferred orientation of the crystals [31]. After adsorbing $NH_{3(g)}$ molecules, **M4**@NH_3 displayed two new quadrupole doublets, while the original quadrupole doublet was maintained (**Figure 8b**), with 41% HS Fe^{II} ions [δ = 1.00(1) mm s^{-1}; ΔE_Q = 2.61(2) mm s^{-1}], owing to the non-porous nature of **M4** resulting in a gradual extension of the sensing process from the crystal surface to the interior. The doublet with blue colour in **Figure 8b** [δ = 0.32(3) mm s^{-1}; ΔE_Q = 0.94(1) mm s^{-1}; A = 33%] is characteristic of LS Fe^{II} ions with a FeN_6 coordination core [24-26] Notably, the isomer shift values agree well with those of the LS sites of reported sensors adsorbing NH_3 (δ = 0.36(3) mm s^{-1}) [27] and (δ = 0.39(3) mm s^{-1}) [24]. A full replacement of the coordination sphere by NH_3 molecules can be ruled out given that $[Fe(NH_3)_6]Cl_2$ shows no quadrupole splitting in their Mössbauer spectra, recorded at room temperature [43]. The other doublet with yellow colour [δ = 0.28(3) mm s^{-1}; ΔE_Q = 0.42(1) mm s^{-1}; A = 26%] is assigned to HS Fe^{III} ions [44], presumably due to air oxidation during the sensing process. The PXRD pattern of **M4**@NH_3 exhibited the characteristic peaks of **M4**, confirming the incomplete character of the transformation (**Figure 8c**). The low diffraction intensity suggests that the new phase formed upon interaction of **M4** with $NH_{3(g)}$ is amorphous. Furthermore, no thermally induced SCO behaviour was observed from the magnetic susceptibility measurement of **M4**@NH_3, the lower $\chi_m T$ value (3.1 cm^3Kmol^{-1}) at 298 K being attributed to the contribution of HS Fe^{III} ions, along with the emergence of LS Fe^{II} ions. Thus, the sensing mechanism of **M4** was ascribed to partial substitution of ligand by the analyte $NH_{3(g)}$ leading to a spin state conversion and partial oxidation from Fe^{II} to Fe^{III} ions. The cyclability was studied by

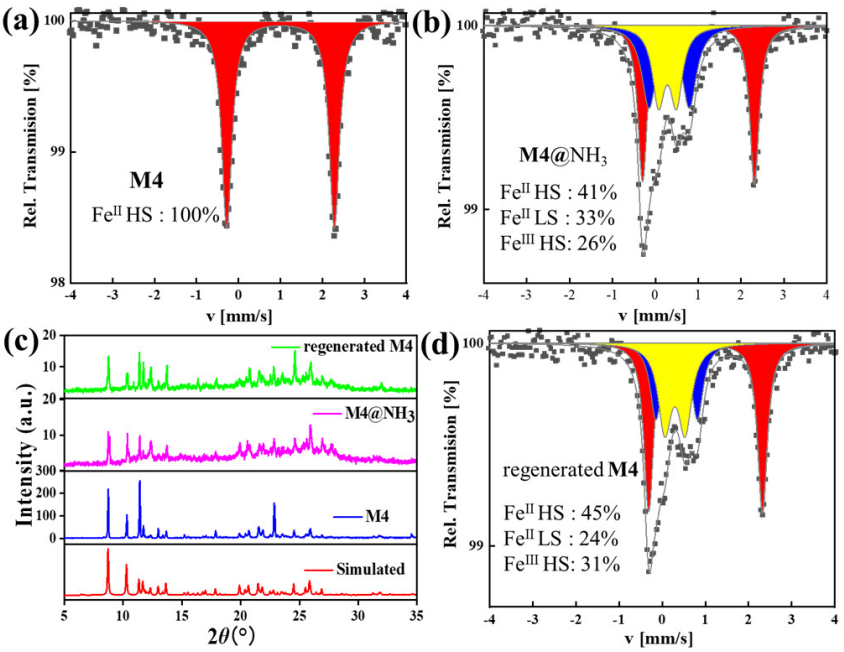


Figure 8. (a) ^{57}Fe Mössbauer spectra of **M4**; **M4**@NH_3 (b) and regenerated **M4** (d), all recorded at room temperature and the red, blue and yellow doublets correspond to HS Fe^{II}, LS Fe^{II} and HS Fe^{III} ions, respectively; PXRD patterns of **M4**, **M4**@NH_3 and regenerated **M4** (c) [39].

heating **M4**@NH_3 overnight in a vacuum at 70 °C and the resulting sample was referred to as regenerated **M4**. The diffuse reflectance spectra and PXRD of regenerated **M4** are in general accordance with those of **M4**@NH_3, indicating that the $NH_{3(g)}$ adsorption-desorption process is irreversible. The ^{57}Fe Mössbauer spectrum of regenerated **M4** exhibited a similar LS Fe^{II}: HS Fe^{II}: HS Fe^{III} (24%: 45%: 31%) ratio to that of **M4**@NH_3 (33%: 41%: 26%) (**Figure 8d**).

The sensing properties were investigated under ambient conditions based on the as-synthesized amorphous SCO cage **1**. As shown in **Figure 9**, **1** can detect $NH_{3(g)}$ within 90 s and the detection process is accompanied by a clear colour variation from light purple to dark grey. The improved response speed compared to **M4** (8 min) is potentially facilitated by the large specific surface area [28.16 m²/g for 1 and 8.37 m²/g for **M4**], which would offer more active sites for ammonia molecules to contact, adsorb, and thus increase the response rate. In addition, the inherent cavity structure of tetrahedral cage **1** (no counter anions inside the cavity detected in the crystal structure) would also increase the diffusion rate of $NH_{3(g)}$, in contrast to the nonporous nature of compound **M4**.

^{57}Fe Mössbauer spectroscopy performed

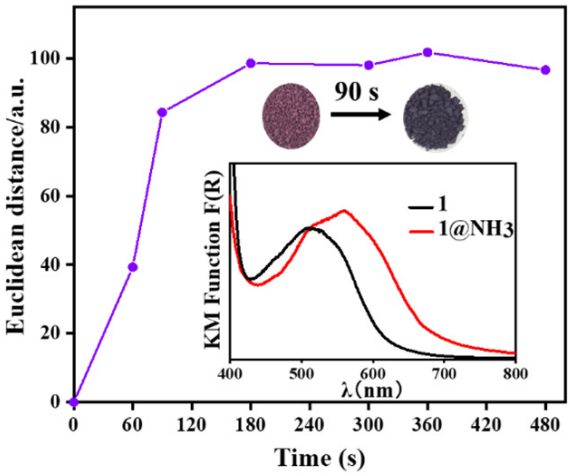


Figure 9. Response time curve of **1** to $NH_{3(g)}$ under vapor diffusion. Inset: diffuse reflectance spectrum and digital images of **1** and **1**@NH_3, KM = Kubelka-Munk [39].

at room temperature was employed to study the sensing mechanism. Three quadrupole doublets were identified in cage **1** (**Figure 10a**). The first doublet HS-1 [δ = 0.95 mm s^{-1}; ΔE_Q = 2.00 mm s^{-1}; A = 24%] with red colour and the second doublet HS-2 [δ = 1.07 mm s^{-1}; ΔE_Q = 2.74 mm s^{-1}; A = 17%] with violet colour correspond to HS Fe^{II} ions. The third doublet with blue colour [δ = 0.37 mm s^{-1}; ΔE_Q = 0.30 mm s^{-1}; A = 59%] is assigned to LS Fe^{II} ions [45]. The LS/HS Fe^{II} ratio is 59 : 41% which at first sight seem to contradict

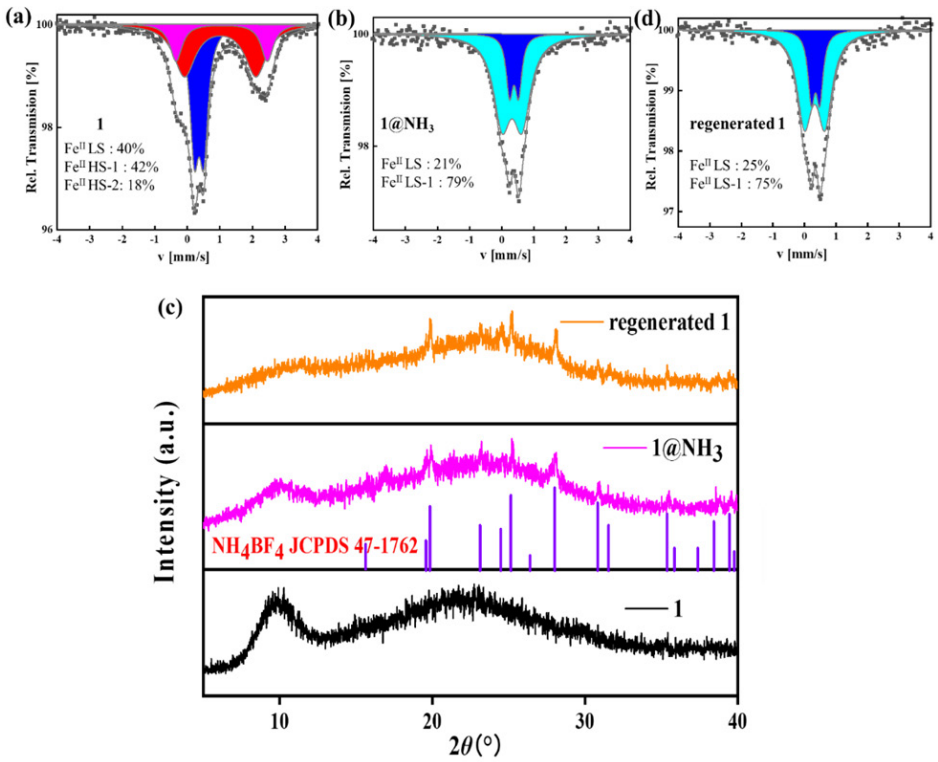
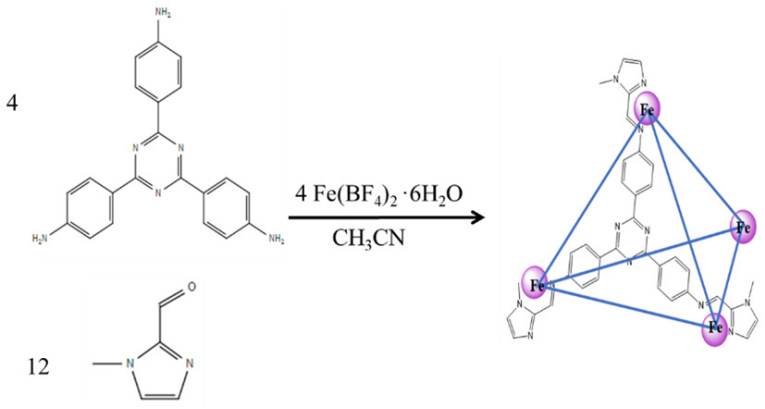


Figure 10. (a) ^{57}Fe Mössbauer spectra of **1**; **1**@NH_3 (b) and regenerated **1** (d), all recorded at room temperature and the red, violet, blue and cyan doublets correspond to HS-1, HS-2, LS and LS-1 Fe^{II} ions; PXRD patterns of **1**, **1**@NH_3 and regenerated **1** (c) [39].

the SQUID and Mössbauer measurements at lower temperatures, since 9.44 $cm^3 \cdot mol^{-1} \cdot K$ at 300 K would correspond to a LS/HS ratio of 1.64 : 2.36 or 41 : 59 % (assuming 4.0 $cm^3 \cdot mol^{-1} \cdot K$ for one HS Fe^{II} ion, see above). The reason for this is that at room temperature the Lamb-Mössbauer factor for LS Fe^{II} can be significantly higher than for HS Fe^{II}, leading to an overestimation of the fraction of LS Fe^{II} from the Mössbauer spectra [46]. Interestingly, after adsorption of $NH_{3(g)}$ molecules, **1**@NH_3 shows only two quadrupole doublets (**Figure 10b**). One doublet marked by blue [δ = 0.38(2) mm s^{-1}; ΔE_Q = 0.27(3) mm s^{-1}; A = 21%] corresponds to LS Fe^{II} from **1**, however another doublet labelled in cyan LS-1 [δ = 0.32(2) mm s^{-1}; ΔE_Q = 0.62(1) mm s^{-1}; A = 79%] is also typical of LS Fe^{II}, indicating that **1** forms a new LS centre after sensing $NH_{3(g)}$ molecules. Notably, the δ and ΔE_Q values are quite similar to those LS Fe^{II} with a FeN_6 core in reported sensors, indicating that $NH_{3(g)}$ is also involved in the coordination of Fe^{II} ions. No traces of Fe^{III} ions were detected in this Mössbauer spectrum, as Fe^{III} HS complexes usually show a quadrupole doublet with δ = 0.25–0.37 mm s^{-1} and ΔE_Q values are relatively small (<0.5 mm s^{-1}), while Fe^{III} LS complexes exhibit δ values in the range of 0.05–0.20 mm s^{-1} and relatively large ΔE_Q values of 1.9–3.0 mm s^{-1} [44]. Another possible origin of the observed LS state would be the formation of hydrogen bonds of both the imine bonds of ligands with ammonia molecules, thus modifying the electronic structure of the sensor [47]. As such, we anticipated that when heating **1**@NH_3 in a vacuum oven, a reversible transition back to the HS state would be observed. As shown in **Figure 10d**, the Mössbauer spectrum of regenerated **1** exhibits two quadrupole doublets similar to **1**@NH_3: [δ = 0.35(1) mm s^{-1}; ΔE_Q = 0.27(3) mm s^{-1}; A = 25%] and [δ = 0.32(2) mm s^{-1}; ΔE_Q = 0.65(1) mm s^{-1}; A = 75%], corresponding to LS and LS-1 Fe^{II} ions. Therefore, given that heating would destroy the hydrogen bonding network, and considering that no major change in spin states and lattice sites was observed after heating, the possibility of hydrogen bonding can be ruled out. The PXRD pattern of **1**@NH_3 also exhibited amorphous humps, but interestingly characteristic peaks of NH_4BF_4 (JCPDS 47-1762) were unambiguously



Scheme 4. Synthesis method of cage **7** [48].

identified, although $Fe(BF_4)_2$•$6H_2O$ was used for the synthesis of **1**. This result indicates that $NH_{3(g)}$ and $H_2O_{(g)}$ molecules first form NH^4+ cations, which then react with BF^4– anions, leading to the formation of NH_4BF_4 during the sensing process (**Figure 10c**). PXRD pattern, diffuse reflectance spectra of regenerated **1** are in general agreement with those of **1**@NH_3, suggesting that the sensing process is irreversible, in line with the analysis of the ^{57}Fe Mössbauer spectra. Hence, based on the above analysis, the sensing mechanism of **1** was attributed to spin state transition of Fe^{II} ions from HS to LS (*i.e.* the formation of a new LS FeN_6 centre) upon intrusion of guest $NH_{3(g)}$ molecules, together with the formation of NH_4BF_4.

In this section, **M4** and cage **1** with different coordination spheres were synthesized. They display different sensing properties of $NH_{3(g)}$ molecules at room temperature. The sensing process can be colorimetrically detected from reddish brown (**M4**) and light purple (**1**) to dark grey. **1** (90 s) exhibits a faster response than **M4** (8 min) due to the presence of the cavity structure and large specific surface area. The sensing mechanism of **M4** is ascribed to the substitution of O-donors of ligands by $NH_{3(g)}$ molecules and partial oxidation of Fe^{II} to Fe^{III}. The sensing mechanism of **1** involves a spin state switching from HS to LS caused by the formation of a new FeN_6 centre and the unprecedented solid-state generation of NH_4BF_4. In addition, the sensing process of $NH_{3(g)}$ is irreversible for **M4** and **1**, because of the modification of the sensor structure, which is promising for applications in colorimetric sensing array technology for $NH_{3(g)}$ sensing.

4. A SCO $Fe^{II}{}_4L_4$ cage for fast ammonia sensing and the monitoring pork spoilage

In section 3, it was learned that although cage **1** and compound **M4** can respond to ammonia, their sensing mechanisms are not the same. Also, quantitative analysis of ammonia gas and further practical applications were not performed. To further investigate the effect of different structures of cages on the sensing mechanism of ammonia gas and to expand the practical use of Fe^{II} complexes-based colorimetric sensors, we designed cage **7** (**Scheme 4**) with $Fe^{II}{}_4L_4$ face-capped configuration and used them as indicators of pork spoilage.

Cage **7** showed a fast response to $NH_{3(g)}$ since the powder turned from light brown to purple in 10 s and kept its colour until 240 s (**Figure 11**). The diffuse reflectance spectrum of **7** exhibited a relatively weak broad band at 530 nm, which is assigned

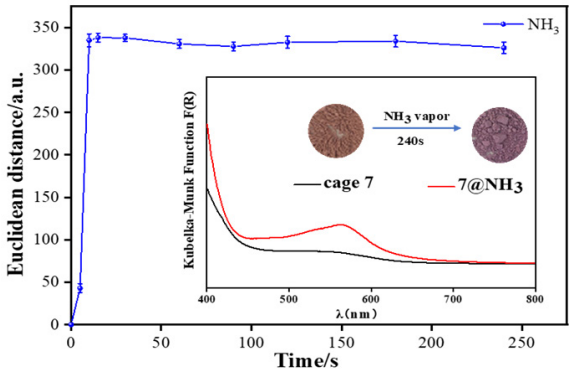


Figure 11. Response time of cage **7** to $NH_{3(g)}$ under vapor diffusion at room temperature. Inset: Diffuse reflectance spectrum and digital photographs of **7** and **7**@NH_3 (exposure for 240 s) [48].

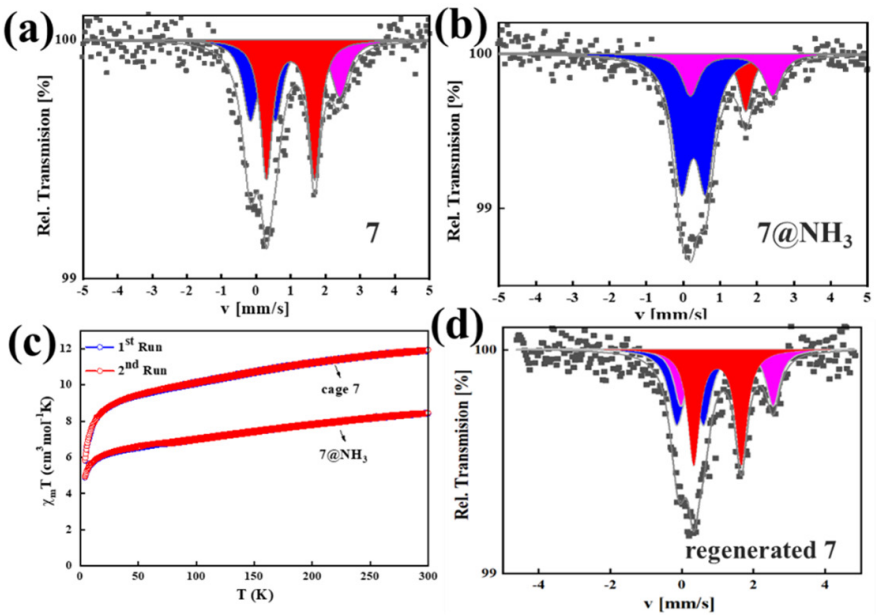


Figure 12. ^{57}Fe Mössbauer spectra of **7** (a), **7**@NH_3 (b) and regenerated **7** (d) recorded at 298 K. The red, magenta and blue quadrupole doublets correspond to HS-1, HS-2 and LS Fe^{II} ions, respectively. (c) Temperature-dependent $\chi_m T$ *vs.* *T* plots for cage **7** and **7**@NH_3 [48].

to metal-to-ligand (MLCT) transition for Fe^{II} centres coordinated to imidazole-imine based ligands [12]. A clear shift of the optical adsorption band can be observed in **7**@NH_3. The high intensity broad band around λ = 565 nm is attributed to the $^1A_1$-$^1T_1$ d–d transition of the LS state in the Fe^{II} compound [23, 25] in agreement with the analysis of ^{57}Fe Mössbauer spectroscopy (discussed later). The improved response speed compared with cage **1** may be attributed to the cavity structure and the large specific surface area (43.8 m²/g), which presumably increases the diffusion rate of $NH_{3(g)}$.

^{57}Fe Mössbauer spectroscopy measurements on **7** and **7**@NH_3 were run to assess the sensing mechanism and probe the spin and oxidation states of this material. The spectrum of **7** reveals three quadrupole doublets (**Figure 12a**). The first one [δ = 0.20(3) mm s^{-1}; ΔE_Q = 0.70(1) mm s^{-1}] is characteristic of low-spin (LS) Fe^{II} ions, with an area fraction (A) of 29%. The two other doublets HS-1 [δ = 0.99(1) mm s^{-1}; ΔE_Q = 1.39(1) mm s^{-1}; A = 44%] and HS-2 [δ = 1.10(4) mm s^{-1}; ΔE_Q = 2.60(1) mm s^{-1}; A = 27%] correspond to high-spin (HS) Fe^{II} ions. The LS/HS Fe^{II} ratio is 29 : 71%. Similar parameters can be found in other Fe^{II} complexes with N_6 donor sets. After sensing NH_3 molecules, the ^{57}Fe Mössbauer spectrum of **7**@NH_3 also exhibits three quadrupole doublets: [δ = 0.27(1) mm s^{-1}; ΔE_Q = 0.66(1) mm s^{-1}; A = 60%]; [δ = 0.96(1) mm s^{-1}; ΔE_Q = 1.45(2) mm s^{-1}; A = 20%]; [δ = 1.29(4) mm s^{-1}; ΔE_Q = 2.19(1) mm s^{-1}; A = 20%], corresponding to LS, HS-1 and HS-2 Fe^{II} ions, respectively (**Figure 12b**). The LS/HS ratio changed significantly to 60 : 40%. No traces of oxidation or oxides were detected up to 10 mm s^{-1} in our spectra. Therefore, the sensing mechanism of cage **7** was ascribed to the transition of the spin state of Fe^{II} ions after intrusion of $NH_{3(g)}$ molecules. On cooling, cage **7** exhibits gradual spin crossover and thermochromic property (**Figure 12c**), which means the ligand field strength can be modified by external stimuli on this system. The $\chi_m T$ undergoes a decrease from 11.92 cm^3•mol^{-1}•K for cage **7** to 8.43 cm^3•mol^{-1}•K for **7**@NH_3 at 298 K, indicating a loss of HS state, which is consistent with the ^{57}Fe Mössbauer spectrum data. The imine linker and triazine ring in the ligands can serve as active sites for NH_3 adsorption, resulting in a change in the electronic structure of the sensor [46, 47]. Thus, we infer that the cause of the spin state transition is caused by the formation of hydrogen bonds between NH_3 molecules and N-rich ligands. PXRD of **7**@NH_3 was not modified confirming the structural integrity. In addition, ^{57}Fe Mössbauer spectroscopy for the regenerated **7** also

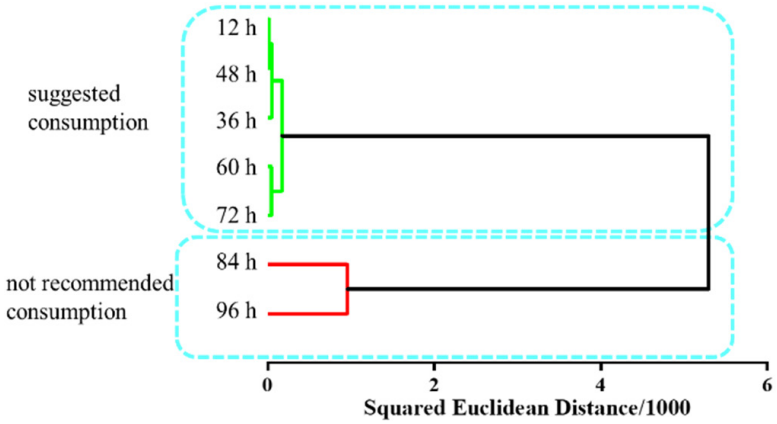


Figure 13. HCA dendrogram for pork spoilage experiment at different time intervals [48].

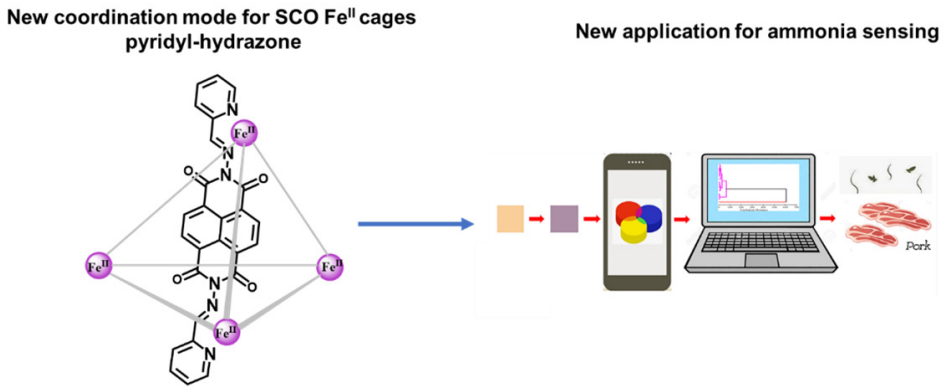
exhibited three quadrupole doublets for LS, HS-1 and HS-2 and the LS/HS Fe^{II} ratio is 33 : 67%, which is almost the same as that of **7** (29 : 71%) (**Figure 12d**). The different sensing mechanisms between cage **1** and **7** may be related to the cage conformations and ligand structures. Cage **7** features a Fe_4L_4 face-capped configuration, whereas **1** presents a Fe_4L_6 edge-bridged configuration. The ligands in **7** are enriched in triazine functional groups, while **1** is enriched in ketone groups. Notably, triazine or nitrogen-enriched ligands can act as adsorption sites for ammonia [46, 47], and alter the electronic structure of the sensor. Therefore, we infer that the interaction of triazine ligands with ammonia could be stronger than that of ketones with ammonia.

Due to the remarkable sensitivity of cage **7**, we thought to use it as an indicator to monitor the spoilage of pork at 4 °C, a typical storage temperature for fresh meat on the shelf. The detailed methodology is provided in the experiment section. At specific time intervals, photographs of the sensor were taken, and these data were treated by HCA. As shown in the dendrogram (**Figure 13**), the data were categorized into two clusters (12–72 h and 84–96 h), indicating that cage **7** presents two different colors on sensing. The results suggest that the meat would be best eaten within 72 h, and starts to spoil at 84 h and is best discarded. A commercial ammonia sensor (AR8500) was used to detect the concentration at each time interval. Considering that there is no clear reference standard for the $NH_{3(g)}$ concentration at each stage of spoilage, the time of rapid concentration increase can be considered as the beginning of the decay process [49]. Before 72 h, no ammonia release was detected by the sensor, indicating that the food was fresh [28]. However, at 84 h and 96 h the concentration of $NH_{3(g)}$ appeared to increase rapidly from 7.8 ppm to 16.4 ppm, indicating that the pork was starting to spoil and was not recommended for consumption, which is consistent with the HCA results [28]. Thus, cage **7** shows great potential in meat safety assessment, be it for food transport or in food storage in household fridges, after opening of the meat packaging.

In this section, a $Fe^{II}_4L_4$ metal organic cage (**7**) with N-rich ligands was successfully prepared for $NH_{3(g)}$ sensing under ambient conditions. The discolouration mechanism is ascribed to the change of the spin state ratio of Fe^{II} ions after adsorption of NH_3 molecules, which possibly are connected to N-rich ligands via hydrogen bonds. Furthermore, we combined colorimetric sensor detection with a smartphone-based analytical method to develop cage **7** as an indicator for monitoring pork meat spoilage at 4 °C, which showed great potential in the field of meat storage and transportation.

General conclusions

Weiyang Li's thesis has reached its two main objectives. The first one was to develop a new coordination mode (pyridyl-hydrazone) to induce SCO behaviour in Fe^{II} tetranuclear cages, without being limited to the conventional coordination modes (imidazole-imine and thiazole-imine) (**section 1 and 2**). The second one was to develop SCO Fe^{II} cages as colorimetric ammonia sensors in the solid



Scheme 5. Schematic representation of the two main objectives in the thesis.

state, not limited to only being porous adsorbents (**Scheme 5**) (**section 3 and 4**). The next research should expand more new coordination modes to induce SCO behaviour, thus diversifying the cage structures. Meanwhile, the sensing performance and mechanism of SCO cages for other toxic and hazardous gas analyses are also worthy of further study.

Acknowledgments

We acknowledge the financial support from Fonds National de la Recherche Scientifique (PDR T.0095.21, CDR J.0064.23) and the China Scholarship Council (201908310083, WL). We thank all our collaborators who contributed to this Ph.D. thesis and whose names are cited in our publication list.

References

(1) Garcia, Y.; Niel, V.; Munoz, M. C.; Real, J. A. Spin crossover in 1D, 2D and 3D polymeric Fe(II) networks. *Spin Crossover in Transition Metal Compounds I* **2004**, 229-257.

(2) Bousseksou, A.; Molnár, G.; Salmon, L.; Nicolazzi, W. Molecular spin crossover phenomenon: recent achievements and prospects. *Chemical Society Reviews* **2011**, *40*, 3313-3335.

(3) Gütlich, P.; Garcia, Y.; Goodwin, H. A. Spin crossover phenomena in Fe(ii) complexes. *Chemical Society Reviews* **2000**, *29*, 419-427.

(4) Halcrow, M. A. Iron(II) complexes of 2, 6-di(pyrazol-1-yl) pyridines—A versatile system for spin-crossover research. *Coordination Chemistry Reviews* **2009**, *253*, 2493-2514.

(5) McConnell, A. J. Spin-state switching in Fe(II) helicates and cages. *Supramolecular Chemistry* **2017**, *30*, 858-868.

(6) Shiga, T.; Tachibana, M.; Sagayama, H.; Kumai, R.; Newton, G. N.; Oshio, H.; Nihei, M. A ring of grids: a giant spin-crossover cluster. *Chemical Communications* **2021**, *57*, 10162-10165.

(7) Hogue, R. W.; Singh, S.; Brooker, S. Spin crossover in discrete polynuclear iron(II) complexes. *Chemical Society Reviews* **2018**, *47*, 7303-7338

(8) Li, W.; Sun, L.; Liu, C.; Rotaru, A.; Robeyns, K.; L. Singleton, M.; Garcia, Y. Supramolecular $Fe^{II}_4L_4$ cage for fast ammonia sensing. *Journal of Materials Chemistry C* **2022**, *10*, 9216-9221.

(9) Wang, Z.; Zhou, L. P.; Cai, L. X.; Tian, C. B.; Sun, Q. F. From a mononuclear FeL_2 complex to a Fe_4L_4 molecular square: designed assembly and spin-crossover property. *Nano Research* **2021**, *14*, 398-403.

(10) Ferguson, A.; Squire, M. A.; Siretanu, D.; Mitcov, D.; Mathonière, C.; Clérac, R.; Kruger, P. E. A face-capped $[Fe_4L_4]^{8+}$ spin crossover tetrahedral cage. *Chemical Communications* **2013**, *49*, 1597-1599.

(11) Bilbeisi, R. A.; Zarra, S.; Feltham, H. L. C.; Jameson, G. N. L.; Clegg, J. K.; Brooker, S.; Nitschke, J. R. Guest binding subtly influences spin crossover in an $Fe^{II}_4L_4$ capsule. *Chemistry – A European Journal* **2013**, *19*, 8058-8062.

(12) Li, L.; Saigo, N.; Zhang, Y.; Fanna, D. J.; Shepherd, N. D.; Clegg, J. K.; Zheng, R.; Hayami, S.; Lindoy, L. F.; Aldrich-Wright, J. R.; Li, C. G.; Reynolds, J. K.; Harman, D. G.; Li, F. A large spin-crossover $[Fe_4L_4]^{8+}$ tetrahedral cage. *Journal of Materials Chemistry C* **2015**, *3*, 7878-7882.

(13) Ren, D. H.; Qiu, D.; Pang, C. Y.; Li, Z.; Gu, Z. G. Chiral tetrahedral iron(ii) cages: diastereoselective subcomponent self-assembly, structure interconversion and spin-crossover properties. *Chemical Communications* **2015**, *51*, 788-791.

(14) Li, L.; Craze, A. R.; Mustonen, O.; Zenno, H.; Whittaker, J. J.; Hayami, S.; Lindoy, L. F.; Marjo, C. E.; Clegg, J. K.; Aldrich-Wright, J. R.; Li, F. A mixed-spin spin-crossover thiozolylimine $[Fe_4L_6]^{8+}$ cage. *Dalton Transactions* **2019**, *48*, 9935-9938.

(15) Zhang, H. X.; Yan, X.; Chen, Y. X.; Zhang, S. H.; Li, T.; Han, W. K.; Bao, L. Y.; Shen, R.; Gu, Z. G. A zeolite supramolecular framework with LTA topology based on a tetrahedral metal–organic cage. *Chemical Communications* **2019**, *55*, 1120-1123.

(16) Han, W. K.; Zhang, H. X.; Wang, Y.; Liu, W.; Yan, X.; Li, T.; Gu, Z. G. Tetrahedral metal–organic cages with cube-like cavities for selective encapsulation of fullerene guests and their spin-crossover properties.

Chemical Communications **2018**, *54*, 12646-12649.

(17) Zhang, F. L.; Chen, J. Q.; Qin, L. F.; Tian, L.; Li, Z.; Ren, X.; Gu, Z. G. Metal-center exchange of tetrahedral cages: single crystal to single crystal and spin-crossover properties. *Chemical Communications* **2016**, *52*, 4796-4799.

(18) Tanaka, T.; Sunatsuki, Y.; Suzuki, T. Synthesis and magnetic properties of tetrahedral tetranuclear iron(II) complexes with bis(bidentate)-type schiff bases containing imidazole groups. *Inorganica Chimica Acta* **2020**, *502*, 119373.

(19) Timmer, B.; Olthuis, W.; Berg, A. v. d. Ammonia sensors and their applications—a review. *Sensors and Actuators B: Chemical* **2005**, *107*, 666-677.

(20) Zhang, D.; Yu, S.; Wang, X.; Huang, J.; Pan, W.; Zhang, J.; Meteku, B. E.; Zeng, J. UV illumination-enhanced ultrasensitive ammonia gas sensor based on (001)TiO_2/MXene heterostructure for food spoilage detection. *Journal of Hazardous Materials* **2022**, *423*, 127160.

(21) Ohtani, R.; Hayami, S. Guest - dependent spin - transition behavior of porous coordination polymers. *Chemistry – A European Journal* **2017**, *23*, 2236-2248.

(22) Gentili, D.; Demitri, N.; Schäfer, B.; Liscio, F.; Bergenti, I.; Ruani, G.; Ruben, M.; Cavallini, M. Multi-modal sensing in spin crossover compounds. *Journal of Materials Chemistry C* **2015**, *3*, 7836-7844.

(23) Naik, A. D.; Robeyns, K.; Meunier, C. F.; Léonard, A. F.; Rotaru, A.; Tinant, B.; Filinchuk, Y.; Su, B. L.; Garcia, Y. Selective and reusable iron(II)-based molecular sensor for the vapor-phase detection of alcohols. *Inorganic Chemistry* **2014**, *53*, 1263-1265.

(24) Guo, Y.; Xue, S.; Dîrtu, M. M.; Garcia, Y. A versatile iron(II)-based colorimetric sensor for the vapor-phase detection of alcohols and toxic gases. *Journal of Materials Chemistry C* **2018**, *6*, 3895-3900.

(25) Sun, L.; Rotaru, A.; Robeyns, K.; Garcia, Y. A colorimetric sensor for the highly selective, ultra-sensitive, and rapid detection of volatile organic compounds and hazardous gases. *Industrial & Engineering Chemistry Research* **2021**, *60*, 8788-8798.

(26) Sun, L.; Rotaru, A.; Garcia, Y. A non-porous Fe(II) complex for the colorimetric detection of hazardous gases and the monitoring of meat freshness. *Journal of Hazardous Materials* **2022**, 437, 129364.

(27) Xue, S.; Wang, L.; Naik, A. D.; Oláh, J.; Robeyns, K.; Rotaru, A.; Guo, Y.; Garcia, Y. Iron(ii) pillared-layer responsive frameworks via “kagomé dual” (kgd) supramolecular tessellations. *Inorganic Chemistry Frontiers* **2021**, *8*, 3532-3546.

(28) Li, W., FeII tetranuclear cages: spin crossover and their ammonia sensing application. *UCLouvain doctoral thesis* 2023.

(29) Li, W.; Liu, C.; Kfoury, J.; Oláh, J.; Robeyns, K.; Singleton, M. L.; Demeshko, S.; Meyer, F.; Garcia, Y. A spin crossover $Fe^{II}_4L_6$ cage based on pyridyl-hydrazone sites. *Chemical Communications* **2022**, *58*, 11653-11656.

(30) Garcia, Y.; Van Koningsbruggen, P. J.; Codjovi, E.; Lapouyade, R.; Kahn, O.; Rabardel, L. Non-classical Fe^{II} spin-crossover behaviour leading to an unprecedented extremely large apparent thermal hysteresis of 270 K: application for displays. *Journal of Materials Chemistry* **1997**, *7*, 857-858.

(31) Xue, S.; Guo, Y.; Rotaru, A.; Müller-Bunz, H.; Morgan, G. G.; Trzop, E.; Collet, E.; Oláh, J.; Garcia, Y. Spin crossover behavior in a homologous series of iron(II) complexes based on functionalized bipyridyl ligands. *Inorganic Chemistry* **2018**, *57*, 9880-9891.

(32) Breuning, E.; Ruben, M.; Lehn, J. M.; Renz, F.; Garcia, Y.; Ksenofontov, V.; Gütlich, P.; Wegelius, E.; Rissanen, K. Spin crossover in a supramolecular Fe^{II}_4[2×2] grid triggered by temperature, pressure, and light. *Angewandte Chemie International Edition* **2000**, *39*, 2504-2507.

(33) Li, W.; Li, X.; Robeyns, K.; Wolff, M.; Kfoury, J.; Oláh, J.; Herchel, R.; Demeshko, S.; Meyer, F.; Garcia, Y. Spin state versatility in $Fe^{II}_4L_6$ supramolecular cages with pyridyl-hydrazone ligand scaffold modulated by solvents and counter anions. *Dalton Transactions* **2024**, *53*, 1449-1459.

(34) Fumanal, M.; Jiménez-Grávalos, F.; Ribas-Arino, J.; Vela, S. Lattice-solvent effects in the spin-crossover of an Fe(II)-based material. The key role of intermolecular interactions between solvent molecules. *Inorganic Chemistry* **2017**, *56*, 4474-4483.

(35) Zheng, J.; von Krbek, L. K. S.; Ronson, T. K.; Nitschke, J. R. Host spin-crossover thermodynamics indicate guest Fit. Angewandte *Chemie International Edition* **2022**, *61*, e202212634.

(36) Scott, A. J.; Vallejo, J.; Sarkar, A.; Smythe, L.; Regincós Martí, E.; Nichol, G. S.; Klooster, W. T.; Coles, S. J.; Murrie, M.; Rajaraman, G.; Piligkos, S.; Lusby, P. J.; Brechin, E. K. Exploiting host–guest chemistry to manipulate magnetic interactions in metallosupramolecular M_4L_6 tetrahedral cages. *Chemical Science* **2021**, *12*, 5134-5142.

(37) Clegg, J. K.; Cremers, J.; Hogben, A. J.; Breiner, B.; Smulders, M. M.; Thoburn, J. D.; Nitschke, J. R. A stimuli responsive system of self-assembled anion-binding $Fe_4L_6^{8+}$ cages. *Chemical Science* **2013**, *4*, 68-76.

(38) Sun, L.; Li, W.; Garcia, Y. ^{57}Fe Mössbauer spectroscopy as a prime tool to explore a new family of colorimetric sensors. Wiley VCH 2024, ch 11, 291-309.

(39) Li, W.; Rotaru, A.; Wolff, M.; Demeshko, S.; Meyer, F.; Garcia, Y. From a mononuclear Fe(ii)L_2 complex to a spin crossover Fe(ii)$_4L_6$ cage by symmetric ligand architecture modification: insights into the ammonia gas sensing mechanism. *Journal of Materials Chemistry C* **2023**, *11*, 11175 - 11184.

(40) Danielsson, P. E. Euclidean distance mapping. *Computer Graphics and image processing* **1980**, *14*, 227-248.

(41) Phonsri, W.; Macedo, D. S.; Vignesh, K. R.; Rajaraman, G.; Davies, C. G.; Jameson, G. N. L.; Moubaraki, B.; Ward, J. S.; Kruger, P. E.; Chastanet, G.; Murray, K. S. Halogen substitution effects on N_2O schiff

base ligands in unprecedented abrupt Fe^{II} spin crossover complexes. *Chemistry – A European Journal* **2017**, *23*, 7052-7065.

(42) Zhang, L.; Xu, G. C.; Xu, H. B.; Mereacre, V.; Wang, Z. M.; Powell, A. K.; Gao, S. Synthesis, magnetic and photomagnetic study of new iron(ii) spin-crossover complexes with N_4O_2 coordination sphere. *Dalton Transactions* **2010**, *39*, 4856-4868.

(43) Bancroft, G. M.; Mays, M. J.; Prater, B. E. The single line mössbauer spectrum of $[Fe(NH_3)_6]^{2+}$. *Chemical Physics Letters* **1969**, *4*, 248-250.

(44) (a) Nihei, M.; Shiga, T.; Maeda, Y.; Oshio, H. Spin crossover iron(III) complexes. Coordination Chemistry Reviews 2007, 251, 2606-2621.(b) Nihei, M.; Ui, M.; Yokota, M.; Han, L.; Maeda, A.; Kishida, H.; Okamoto, H.; Oshio, H. Two - step spin conversion in a cyanide-bridged ferrous square. *Angewandte Chemie International Edition* **2005**, *117*, 6642-6645.

(45) Gütlich, P.; Bill, E.; Trautwein, A. X.: *Mössbauer spectroscopy and transition metal chemistry: fundamentals and applications*; Springer Science & Business Media, 2010.

(46) Niu, F.; Shao, Z. W.; Zhu, J. L.; Tao, L. M.; Ding, Y. Structural evolution of imine-linked covalent organic frameworks and their NH_3 sensing performance. *Journal of Materials Chemistry C* **2021**, *9*, 8562-8569.

(47) Niu, F.; Shao, Z. W.; Tao, L. M.; Ding, Y. Covalent triazine-based frameworks for NH_3 gas sensing at room temperature. *Sensors and Actuators B: Chemical* **2020**, *321*, 128513.

(48) Li, W. ; Sun, L. ; Liu, C. ; Rotaru, A. ; Robeyns, K. ; Singleton, M. L.; Garcia, Y. *J Journal of Materials Chemistry C* **2022**, *10*, 9216 - 9221.

(49) Cai, C.; Mo, J.; Lu, Y.; Zhang, N.; Wu, Z.; Wang, S.; Nie, S. Integration of a porous wood-based triboelectric nanogenerator and gas sensor for real-time wireless food-quality assessment. *Nano Energy* **2021**, *83*, 105833.

Future Conferences, Symposia, Workshops

August 14- 16, 2025
16th National Conference on Mössbauer Spectroscopy
Dalian, China
https://wangjh.dicp.ac.cn/info/1090/3142.htm (Chinese)
https://wangjh.dicp.ac.cn/info/1119/3143.htm (English)

September 7 - 12, 2025
ICAME & HYPERFINE 2025 38th International Conference on the Applications of the Mössbauer Effect, ICAME, and the International Conference on Hyperfine Interactions and Their Applications, HYPERFINE
Gdańsk, Poland
https://icame-hi-2025.pollub.pl/